Deliverable D 2.6
Input for the simulation of thermal and mechanical behaviour of joints

Document type	**Deliverable D 2.6**
Document Version / Status	**1.6**
Primary Authors	**João Pereira, jpereira@civil.uminho.pt, UMINHO**
Distribution Level	**PU (Public)**
Project Acronym	**ATHOR**
Project Title	**Advanced THermomechanical multiscale mOdelling of Refractory linings**
Grant Agreement Number	**764987**
Project Website	www.etn-athor.eu
Project Coordinator	**Marc Huger, marc.huger@unilim.fr, UNILIM**
Document Contributors	**João Pereira, jpereira@civil.uminho.pt, UMINHO** **Alain Gasser, alain.gasser@univ-orleans.fr , UORL** **Mahmoud Ali, mahmoud.ali@univ-orleans.fr, UORL** **Rafael Oliveira, rafael.oliveira@uc.pt, UMINHO** **Pratik Gajjar, pratik.gajjar@civil.uminho.pt, UMINHO**

History of Changes

Version	Date	Author (Organization)	Change	Page
1.0	02.06.2021	Rafael Oliveira	First version of the Deliverable created Data for dry joint	All
1.1	10.06.2021	Mahmoud Ali Pratik Gajjar	Data for mortared joints Data for dry joint at high temperature	All
1.2	15.06.2021	Alain Gasser	Review	All
1.3	20.06.2021	João Pereira	Review	All
1.4	25.06.2021	Glyn Derrick	English check and formatting	All
1.5	29.06.2021	João Pereira Alain Gasser Mahmoud Ali Pratik Gajjar Marc Huger	Final corrections and check	All
1.6	30.06.2021	Pratik Gajjar Glyn Derrick	Minor corrections	5-9

Horizon 2020
European Union funding
for Research & Innovation

TABLE OF CONTENTS

1 Introduction

This report will gather the experimental data regarding the mechanical behaviour of joints as a specific component of the refractory lining within the steel ladle. The data from this report will be used in the numerical simulations within WP3. The results presented in this document come from experimental campaigns developed at University of Coimbra, TataSteel and University of Orléans. The experimental campaigns at University of Coimbra and TataSteel focuses on dry joint (without mortar) behaviour. Here, the objective is to study the behaviour of the working lining of the model steel ladle (Figure 1), which is composed of dry-stacked alumina spinel bricks. The experimental campaigns at University of Orleans focuses on joints with mortar. Here, the objective is to study the behaviour of the safety lining of our model steel ladle (Figure 1). The experimental characterization of the joints includes characterization at ambient and high temperatures.

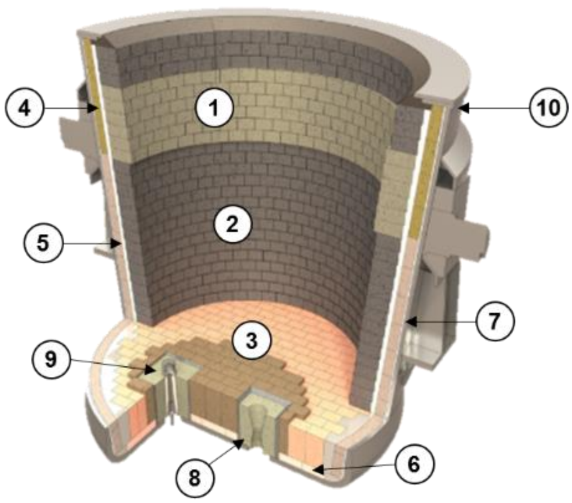

		Lining Zone
1	Working Lining	Slagzone
2		Barrel
3		Bottom/Impact pad
4	Safety Lining	Slagzone
5		Barrel
6		Bottom
7		Insulation
8	Casting system	
9	Stirring system	
10	Steel Shell	

Figure 1 – Schematic representation of a steel ladle.

European Commission
Horizon 2020
European Union funding
for Research & Innovation

2 Typical joint behaviour modelling

In a masonry, joints can be sollicitated in tension, compression and shear. Dry joints and mortar joints present some diffences in their behaviour under these sollicitations. For mortar joints, the joint stiffness is given by the mortar stiffness. For dry joints, the stiffness is given by the evolution of the contact pressure versus the joint overclosure (due to the progressive gap closure between bricks during compression loading). Another important part of their behaviour is their strength. Their shear-compression strength can be described by a Mohr-Coulomb yield function:

$$f(\tau, \sigma_n, \Phi) = |\tau| - C + \sigma_n \tan\, \Phi \qquad \text{Equ. 1}$$

Where τ, σ_n and Φ are the shear stress, normal stress and the internal friction angle. C is the cohesion of the material.

To take into account the strength in tension, a tension strength f_t is added. The global yield surface in shown on Figure 2. For mortar joints, this surface represents the failure of the brick/mortar interface or of the mortar.

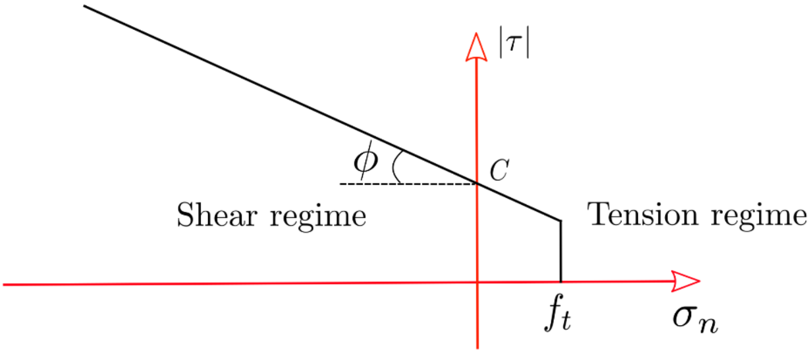

Figure 2 - 2D space representation of the yield surface of the brick-mortar interface (Brulin et al. 2020).

In the case of dry joints, joints have no cohesion (*c=0*) and have no tensile strength (f_t=0) because a dry joint opens under tension (Figure 3).

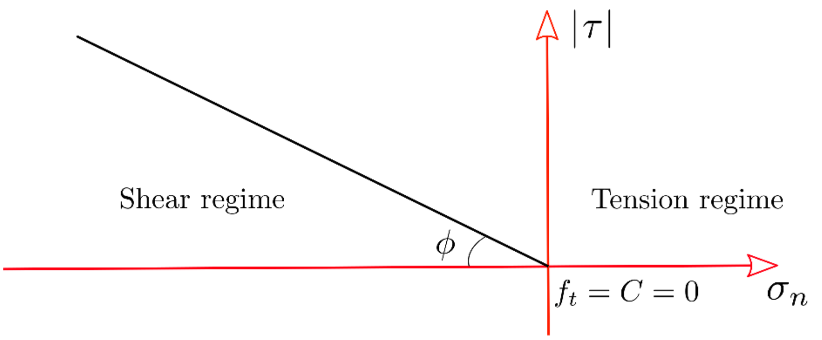

Figure 3 - 2D space representation of the yield surface of dry joints.

To identify the parameters of these different joint behaviours at different temperatures, it is necessary to perform several types of tests:

- For dry joints: compression tests of two bricks to obtain the normal behaviour (contact pressure versus joint overclosure), and friction tests to identify the shear behaviour (Φ)
- For mortar joints: slant shear tests for shear compression behaviour (C and Φ), and tensile tests for tensile behaviour (f_t).

3 Dry joints (without mortar)

The experimental characterization of dry joints (without mortar) was performed at University of Coimbra and included characterization of the normal behaviour and shear behaviour.

3.1 Normal behaviour

This section presents the characterization of the normal behaviour of the joint, based on experimental campaigns developed at University of Coimbra and TataSteel. It includes classical joint closure tests, at ambient and high temperatures, and measurement and analyses of the heterogeneity of the joints in a wallet using DIC.

3.1.1 Classical joint closure test

The joint closure test allows to assess the normal behaviour of the dry joints. In this test, two stacked bricks are compressed, and the displacements are recorded (Gasser et al, 2004; Andreev et al, 2012; Allaoui et al, 2018). The joint thickness may be obtained based on the force-displacement diagram.

3.1.1.1 Experimental setup

For this experimental campaign, the adopted specimens consisted of a masonry prism composed of only two stacked bricks with a dry joint. The bricks were cut using a circular diamond saw, and the final dimensions of the bricks composing the specimen were 124 × 124 mm by 76 mm in height. When building the specimen, the original face of the brick was used at the joint. The final dimensions of the prism were 124 × 124 mm by 152 mm in height. These joint closure tests were performed at ambient temperature. A multipurpose Servo Hydraulic Universal Testing Machine W+B Series LFV (maximum capacity of 600 kN) was used (Figure 4a). The displacements were measured with an Epsilon extensometer measuring the relative displacement of steel supports glued to the specimen (Figure 4b). A compressive load was applied under load control at the constant rate of 0.5 kN/s, up to 150 kN. At this load level, the average compressive stress was 9.76 MPa and a linear behaviour was expected at the bricks. The thickness of the joints was estimated based on the force-displacement curve obtained in the joint closure test, considering the intersection of the linear section of the curve, with the horizontal axis in the plot (Gasser et al, 2004). Three load cycles were applied to the specimen.

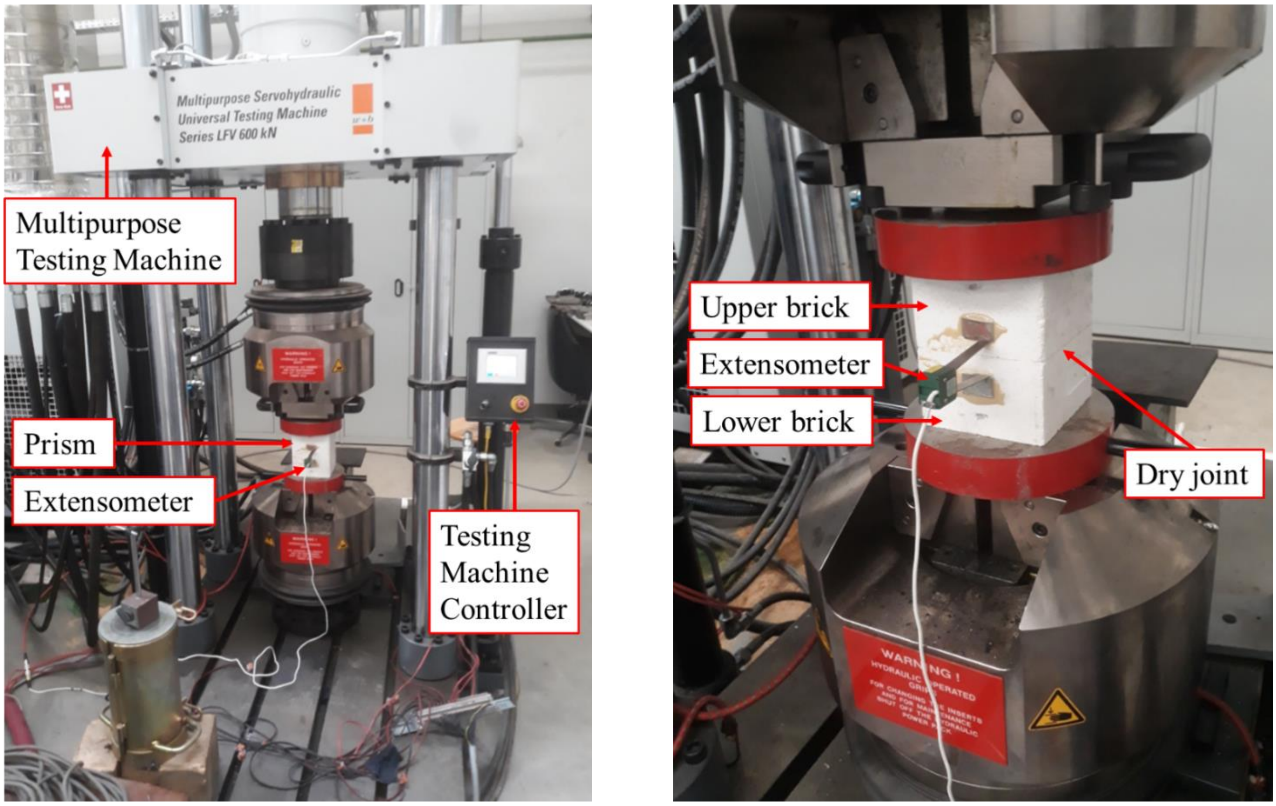

a) b)

Figure 4 – Joint closure test - Experimental setup: a) Overview and b) Details of prism and extensometer.

3.1.1.2 Results and discussion

The results of the joint closure tests are given in Figure 5. At the first cycle, it is possible to identify a behaviour, which is different from the behaviour of the subsequent cycles due to adjustment of the contact surface at the joint. The initial joint thickness was 0.022 mm. For the second and third load cycles, a more similar behaviour was observed and the joint thickness reduced then to 0.007 mm. This reduction is caused by joint degradation due to crushing of initial non-flat surfaces of the bricks. This happens along the first load cycle, as observed by other researchers (Allaoui et al, 2018; Gasser et al, 2004; Andreev et al, 2012; Prietl, 2006; Prietl et al, 2006). The joint degradation increases the contact area between the bricks, leading to an increase of the initial stiffness of the prism.

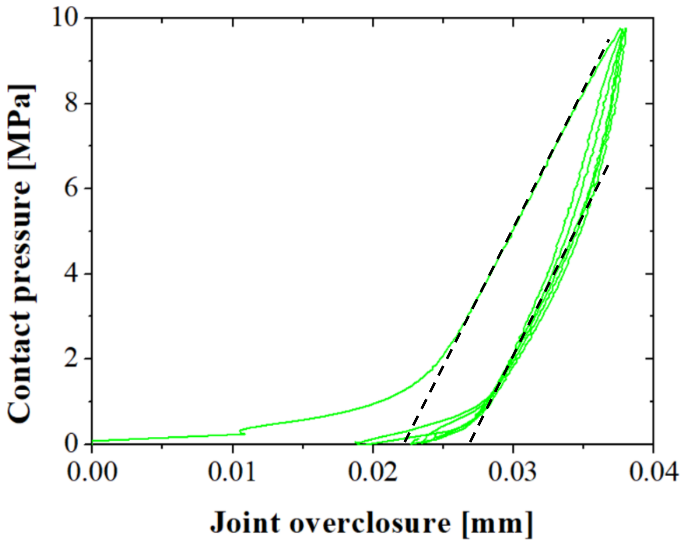

Figure 5 – Joint overclosure curve.

3.1.2 Joint closure test at high temperature

For the assessment of the joint behaviour at high temperatures, an experimental campaign was developed at TataSteel. Joint closure tests on cylindrical specimen of alumina spinel bricks were performed to observe its behaviour at different high temperatures.

3.1.2.1 Experimental setup

Cylindrical specimens were chosen for these tests as the furnace used alongside the testing machine was not large enough to allow the testing of entire bricks. The experimental setup adopted for these tests was similar to that in the previous section. The specimens were obtained by coring the bricks, the final dimensions of the specimens were 50 mm in diameter and 50 mm in height. A Zwick Z250 material testing machine (maximum capacity 250 kN) was used for these tests (Figure 6a). The displacements were measured using Maytec extensometer at room temperature and LVDT attached for crosshead travel at high temperatures (Figure 6b).

A compressive load was applied using displacement control at the constant rate of 0.005 mm/s, up to 35 kN. At this load level, the average compressive stress in specimen was 18 MPa and an elastic behaviour was expected in the bricks. For the tests at high temperature a pre-load of 0.3 kN was applied during the heating period to keep the specimen aligned while the desired temperature is achieved.

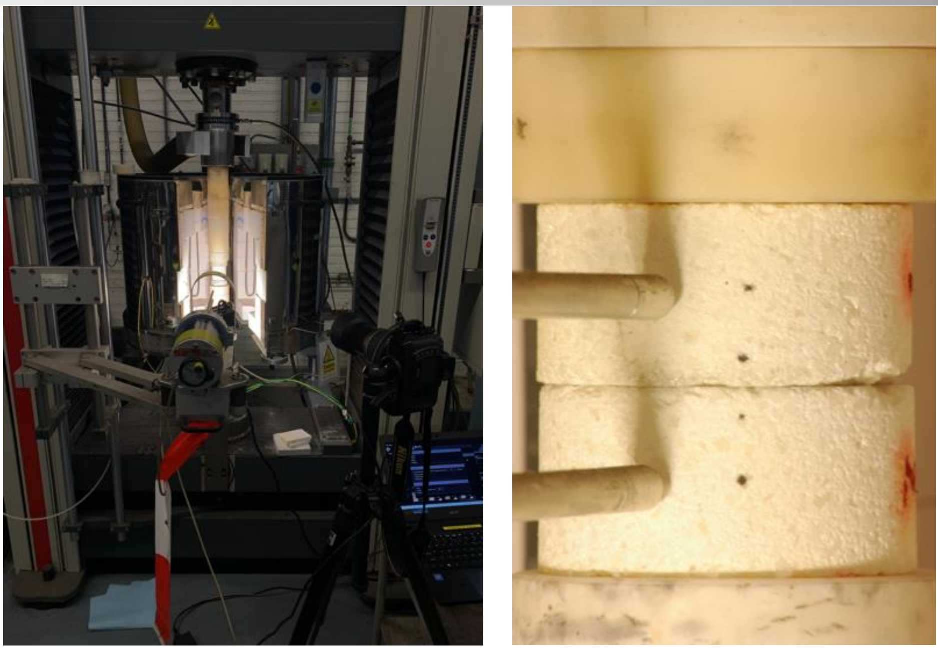

a) b)

Figure 6 – Joint closure test at high temperature - Experimental setup: a) Overview and b) Details of prism and extensometer.

3.1.2.2 Results and discussion

To evaluate the joint closure behaviour, a reference specimen (i.e. a specimen without any joints) was tested and the loading-unloading behaviour of the reference and specimen with dry joints were compared. Figure 7 presents the behaviour observed for these specimens at 20 ºC. From the figure, it can be observed that, for the specimen with a dry joint, the initial displacement at lower contact pressure is high and, as the pressure increases, the displacement reduces. This is classic behaviour for dry joints at lower level of pressure. This results from the fact that the contact area between the two surfaces of a dry joint is less than the total surface area due to presence of surface asperities. As the load increases, these asperities are crushed, due to the high stress concentration, which ultimately increases the contact area. As a consequence of this increased contact area, displacement between the specimen reduces.

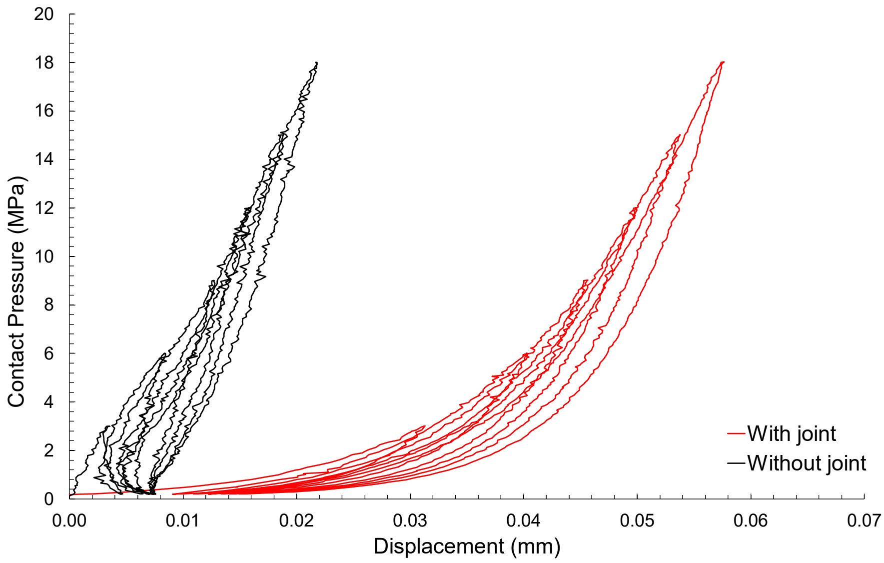

Figure 7 – Joint closure test results at 20 ºC.

From Figure 7, it can be seen that the response obtained for both the samples at higher contact pressure is similar indicating, that at higher pressure levels, the joints are closed. It also can be observed that the loading and unloading response of specimen with joint at high pressure level is similar to the response observed for the specimen without a joint. To calculate the joint thickness and the stress at which it closes, the elastic response during loading of the specimen without joint can be subtracted from the loading behaviour observed for the specimen with a joint.

Figure 8 shows the joint behaviour at 20 ºC. The behaviour of dry joint is obtained via the subtraction the elastic response of the specimen without a joint, from the response of specimen with a joint. From the test performed at 20 ºC, it can be observed that the joint closes at 0.037 mm during the loading, which can be classified as its joint thickness. However, it can also be observed that the joint does not close completely even at high pressure and there is still a residual value of joint thickness that can be observed during the unloading and reloading. In this case, the value of residual joint thickness was observed to be 0.0095 mm.

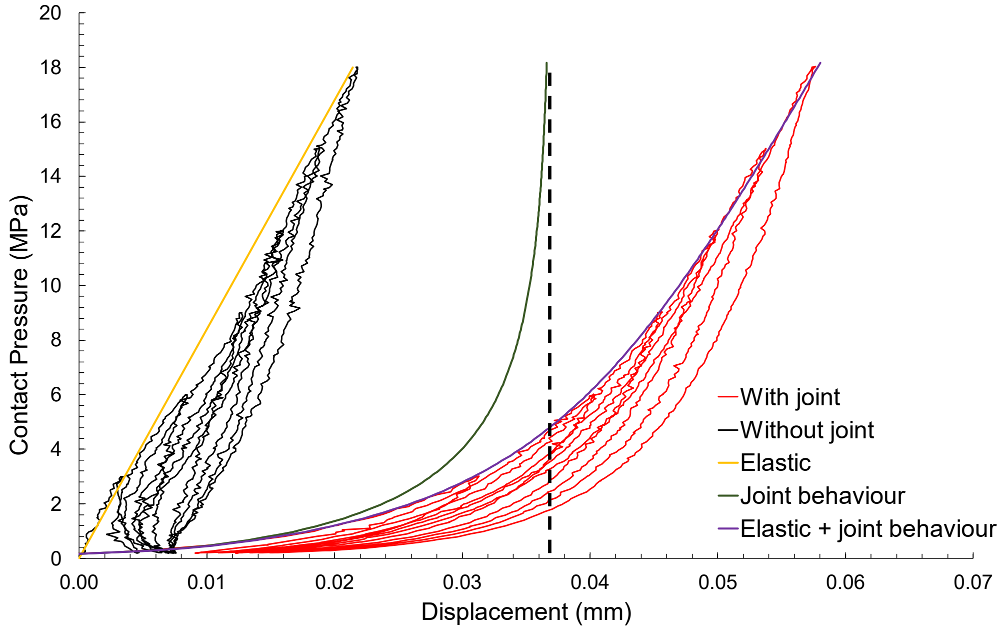

Figure 8 – Joint behaviour at 20 ºC.

The same approach was taken for the tests at eleveated temperatures. The results of the joint closure tests are given in Figure 9. The tests were performed at 600 ºC, 800 ºC, 1000 ºC and 1200 ºC. The behaviour observed in these tests was similar to that observed for the test performed at 20 ºC (i.e. for lower presure, high displacement that reduces as the pressure increases).

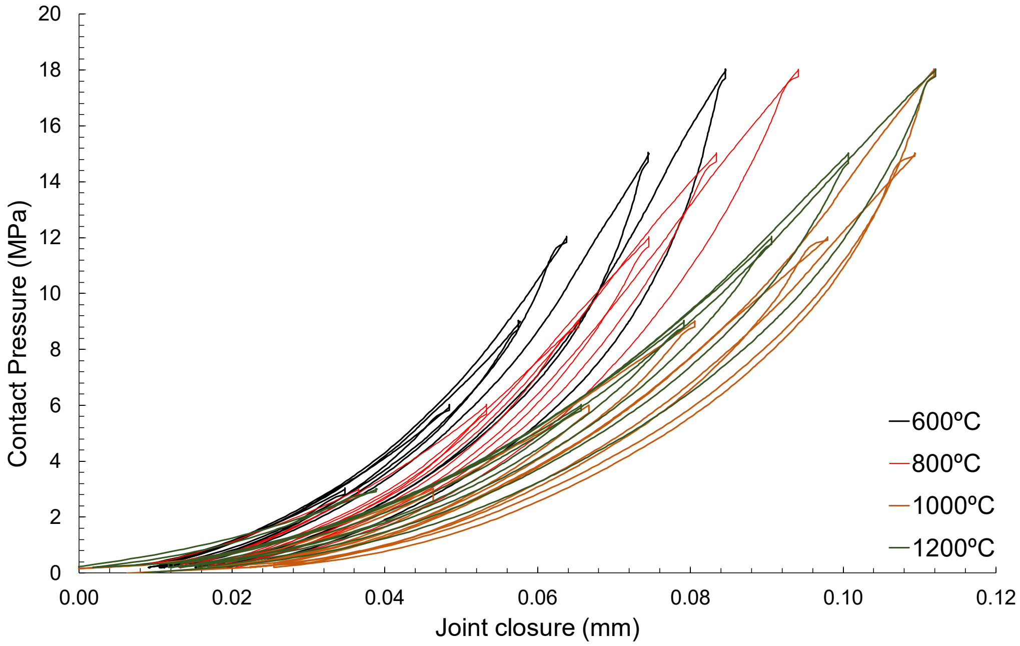

Figure 9 – Joint closure test results at high temperatures

The joint closure behaviours, at these elevated temperatures, are obtained using the same process used for the results obtained at 20 ºC and are presented in Figure 10. No major change in the joint thickness was observed with respect to the increasing

European Commission | Horizon 2020 European Union funding for Research & Innovation

temperature, however, it can be noted that, as the temperature increases, the contact pressure required to close the joint decreases.

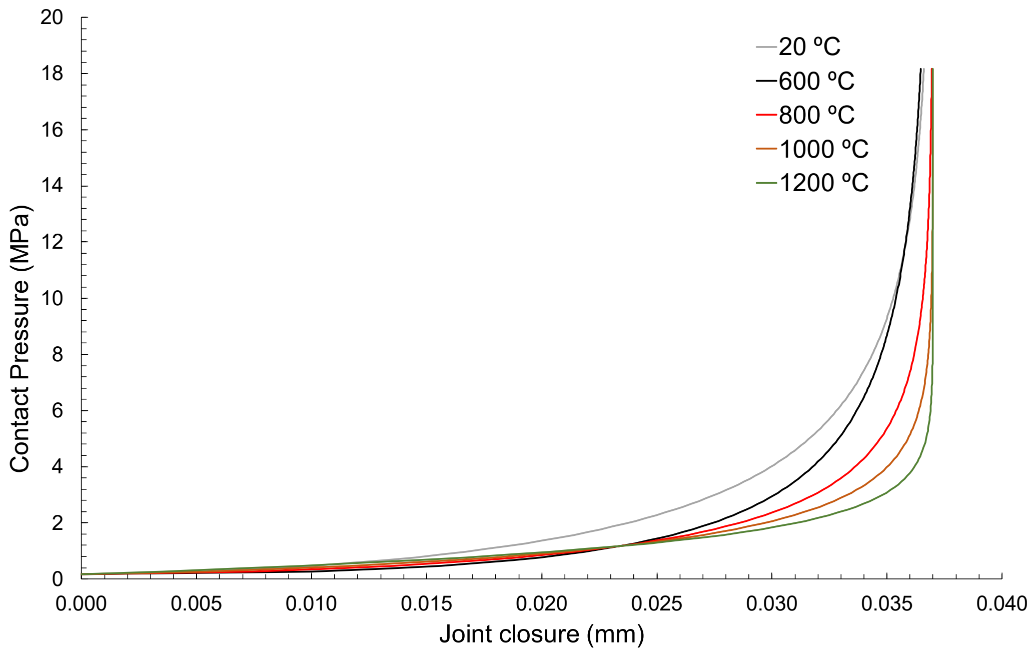

Figure 10 – Joint closure behaviour at high temperatures.

3.1.3 Heterogeneity in joint behaviour

In addition to the imperfections of the contact surface, that could be revealed by the two previous tests (using only two bricks), when bricks are dry stacked to form a masonry wallet, closure mechanisms of all joints of the assembly could also be greatly affected by shape imperfections of the bricks: non-regular parallelepipeds, non-parallel surfaces and non-uniform thicknesses. In such a situation, it is impossible to avoid the creation of additional gaps between bricks. Consequently, such a configuration has a significant impact on the load transfer through the masonry, involving different stress levels on each brick. In order to assess individual joint behaviour within such masonry wallets, the behaviour of the joints has been monitored during loading in uniaxial compression. Details regarding the experimental device will be provided in Deliverable 4.3. In the present deliverable, only the results regarding this joint behaviour are assessed (Figure 11).

Joint closure curves, at different points, were obtained using DIC (Figure 12a). Figure 12b presents the curves for different points in the wall and is compared with the curve obtained in the classical joint closure test. It is thus possible to identify a significant scattering on the curves obtained by DIC in different locations. Some joints (for example P9) behave similarly to the classical joint closure test and some others (for example P11) behave very differently indicating a huge initial gap (typically up to 0.2 mm). This is a direct result of the different loading conditions on each brick, induced by their shape imperfections. Consequently, the shape imperfections of the bricks result in larger initial joint thicknesses and has a considerable influence on the joint behaviour. The obtained results suggest that careful use of the data from the classical joint closure test is required as the initial joint thickness measured in a single joint may deviate significantly from the one present in masonry walls or panels.

European Commission | Horizon 2020 European Union funding for Research & Innovation

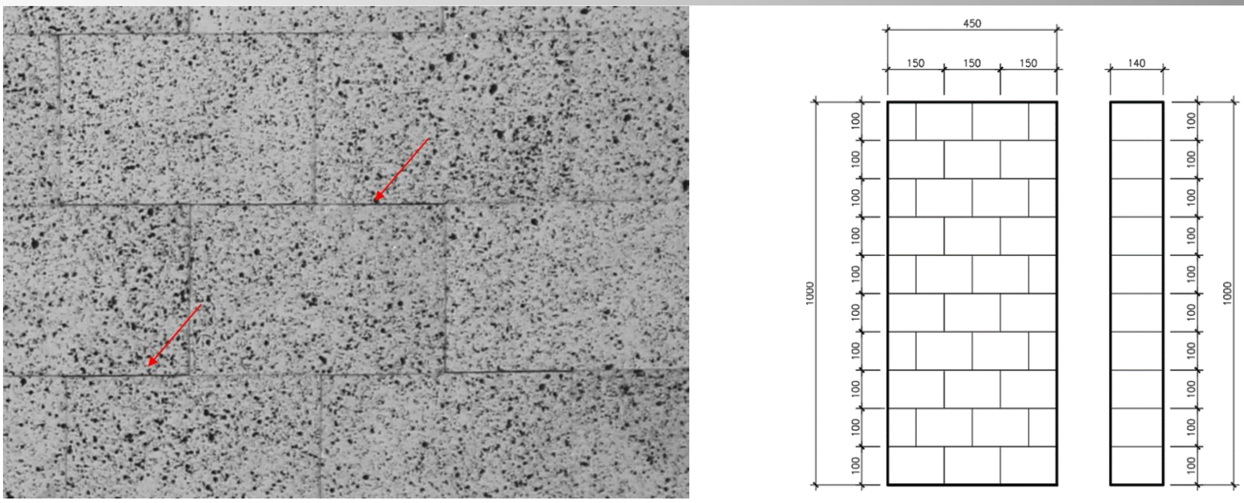

a) b)

Figure 11 – Dry stacked masonry wallet: a) Bed joints imperfections in mortarless refractory masonry as well as speckle preparation for DIC measurements and b) Dimensions of the masonry wallet.

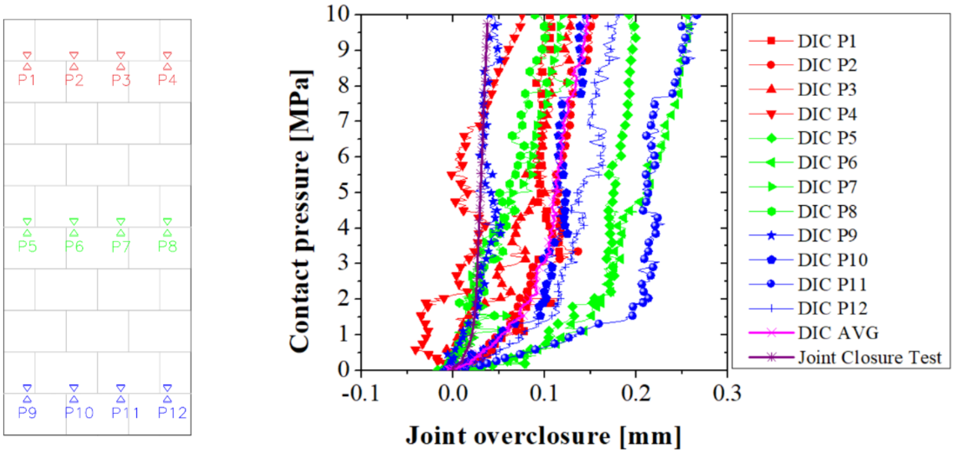

a) b)

Figure 12 – Heterogeneity in joint's normal behaviour: a) Locations and b) Joint overclosure curves.

3.2 Shear behaviour

The shear behaviour of joints in masonry is ruled by the Coulomb friction law (Gasser et al, 2004; Nguyen et al, 2009). The part 3 of EN 1052-3 (2002) is widely used to determine the initial shear strength at ambient temperature for joints with mortar. The triplet shear tests may be also used to characterize dry joints. However, it is a challenge to perform this test at high temperatures, as it requires the application of loads in two orthogonal directions. The Slant Shear test was successfully used to characterize the brick/mortar interface at ambient and high temperatures (Brulin et al, 2020), however, the slant shear test cannot be used in the case of dry joints. When dealing with mortarless masonry, only the friction coefficient (or friction angle) needs to be identified. A simple test is the use of an inclined plane, with increasing rotation, this makes it possible to measure the initial angle of sliding (Gasser et al, 2004). This slip test can be easily adapted to be performed at high temperatures. A dedicated device was developed in this research to evaluate the friction angle of dry joints at ambient and high temperatures. The experimental characterization of the tangential behaviour of dry-joints comprised fifteen tests performed at ambient and high temperatures divided in four series (Table 1).

Table 1 – Test series – Slip Test

Series	Specimen	Testing temperature
ST.RT	ST.RT.01.A	Ambient temperature
	ST.RT.01.B	
	ST.RT.01.C	
	ST.RT.02.A	
	ST.RT.02.B	
	ST.RT.02.C	
ST.300	ST.300.01	300 °C
	ST.300.02	
	ST.300.03	
ST.600	ST.600.01	600 °C
	ST.600.02	
	ST.600.03	
ST.900	ST.900.01	900 °C
	ST.900.02	
	ST.900.03	

3.2.1 Experimental setup

In this newly developed slip test setup, a tilting beam was positioned inside an electrical furnace with a pinned support. A hydraulic jack, connected to the beam by a load rod, was used to increase the inclination of the beam. Two stacked bricks were positioned on the device, the bottom brick was constrained by steel plates, but the upper brick was allowed to move (Figure 13). When the hydraulic jack moves upward, it increases the inclination of the beam, from zero degrees up to the friction angle of the joint (Figure 13b).

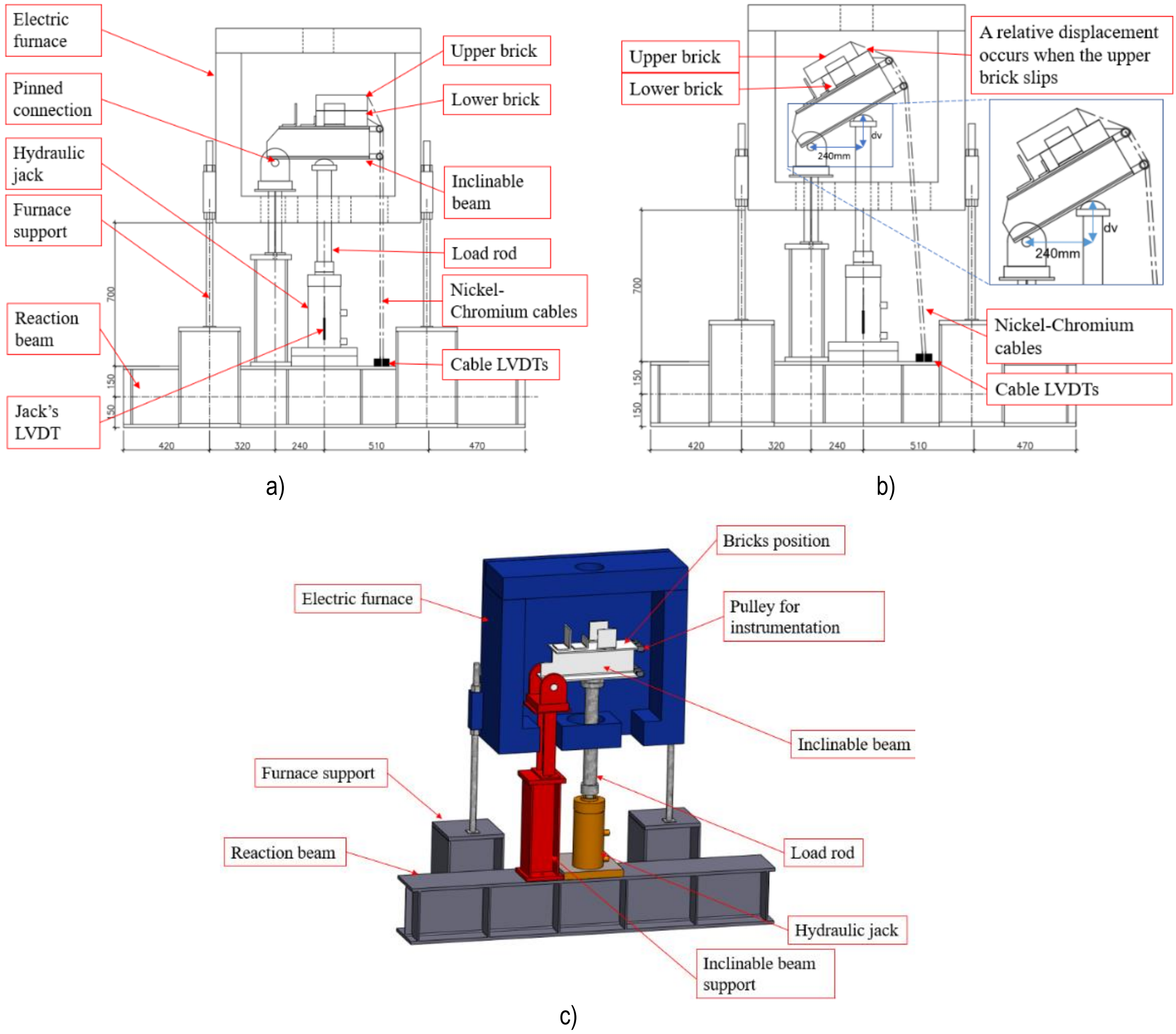

Figure 13 – Slip test scheme: a) before slipping, b) after slipping and c) 3D model.

A picture of the experimental setup is presented in Figure 14. A W+B servo controlled hydraulic unit was used to control the hydraulic jack. The data was acquired using a TML TDS-601 datalogger. In order to avoid overheating of the inclinable beam and hydraulic jack, ceramic wool was used to protect the steel components from high temperatures. Moreover, a cooling device was used to cool the load rod, avoiding excessive temperatures in the hydraulic jack. Two LVDT cables were used to measure the displacement of the bottom brick and one LVDT cable was used to monitor the displacement of the upper brick. The LVDTs were connected to the bricks using Nickel-Chromium cables in order to avoid the influence of their thermal elongation (Figure 15). When the upper brick slips, a differential displacement between these LVDTs is registered. A rod LVDT was used to measure the displacement of the hydraulic jack and another one was used to feed the servo controller unit. The details of the LVDTs are presented in Figure 16.

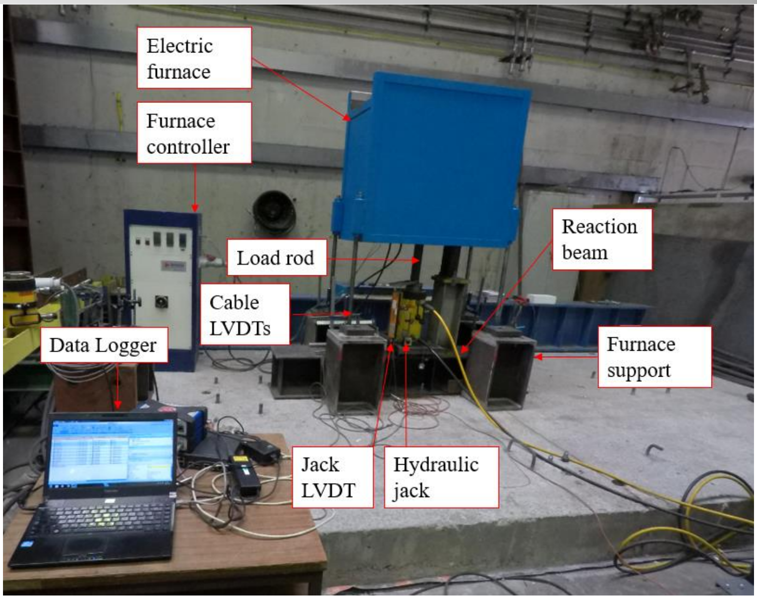

Figure 14 – General view of the slip test experimental set-up.

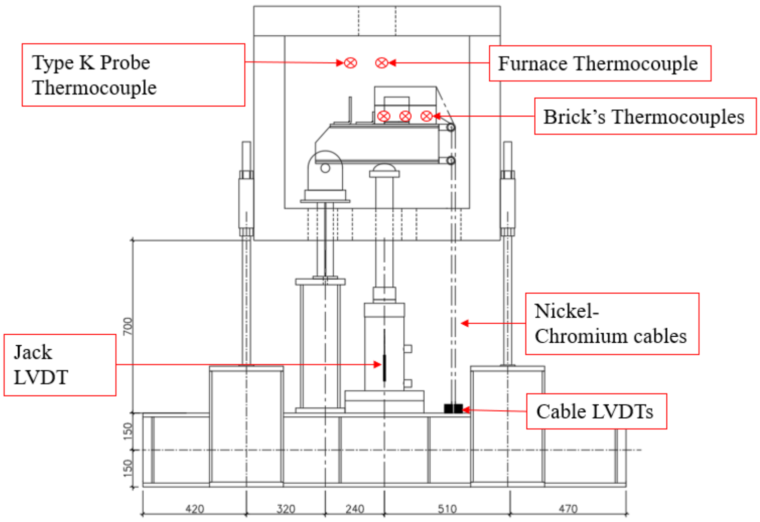

Figure 15 – Slip test instrumentation: LVDTs and thermocouples.

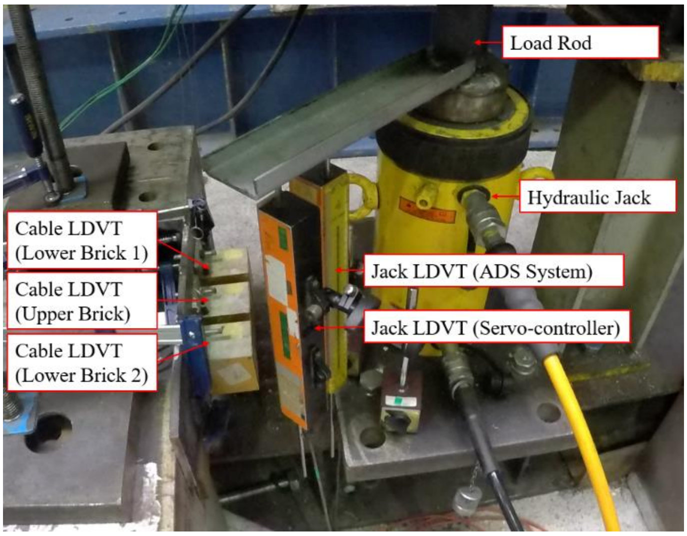

Figure 16 – Slip test instrumentation: LVDTs – Details.

The friction angle (ø) between the bricks may be calculated by the arctangent of the vertical displacement measured at the jack (d_v) divided by the offset between the axis of the jack and the axis of the hinge (Figure 13b), as shown in Equ. 2:

$$ø = \text{atan}\,(d_v / 240\text{mm}) \qquad \textbf{Equ. 2}$$

The furnace had built-in type K thermocouples for controlling the temperatures, but an additional type K probe thermocouple was used to measure the temperatures in the furnace during the test. Additionally, three type K wire thermocouples were used to measure the temperatures inside the brick (Figure 17).

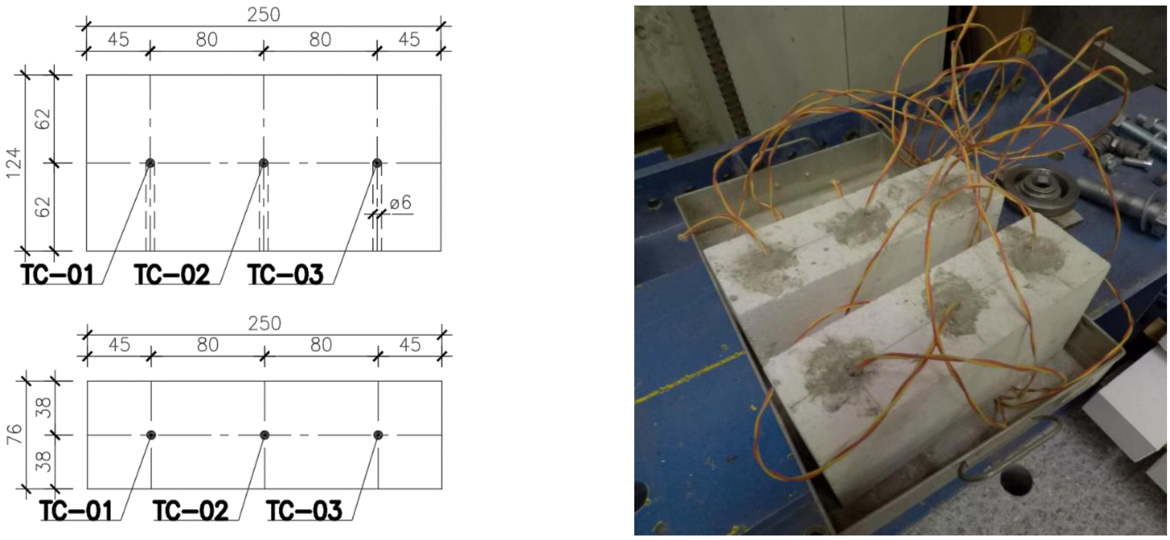

a) b)

Figure 17 – Thermocouples embedded in the bricks: a) Position and b) Specimens.

The specimens consisted of two stacked bricks of type *B* (250×124×76 mm), therefore the final dimensions of the prism were 250×124×152 mm (Oliveira et al, 2019). The prism can be seen in Figure 18.

Figure 18 – Prism composed by two stacked bricks inside the furnace chamber.

In order to confirm that the temperature was homogenized within the specimen, the bottom brick had thermocouples. Figure 19 shows the position of the thermocouples installed in the specimens and the development of the temperature in the specimens. As can be seen in the figure, at the time of the application of the mechanical load (after the heating) the specimen was under homogeneous temperature.

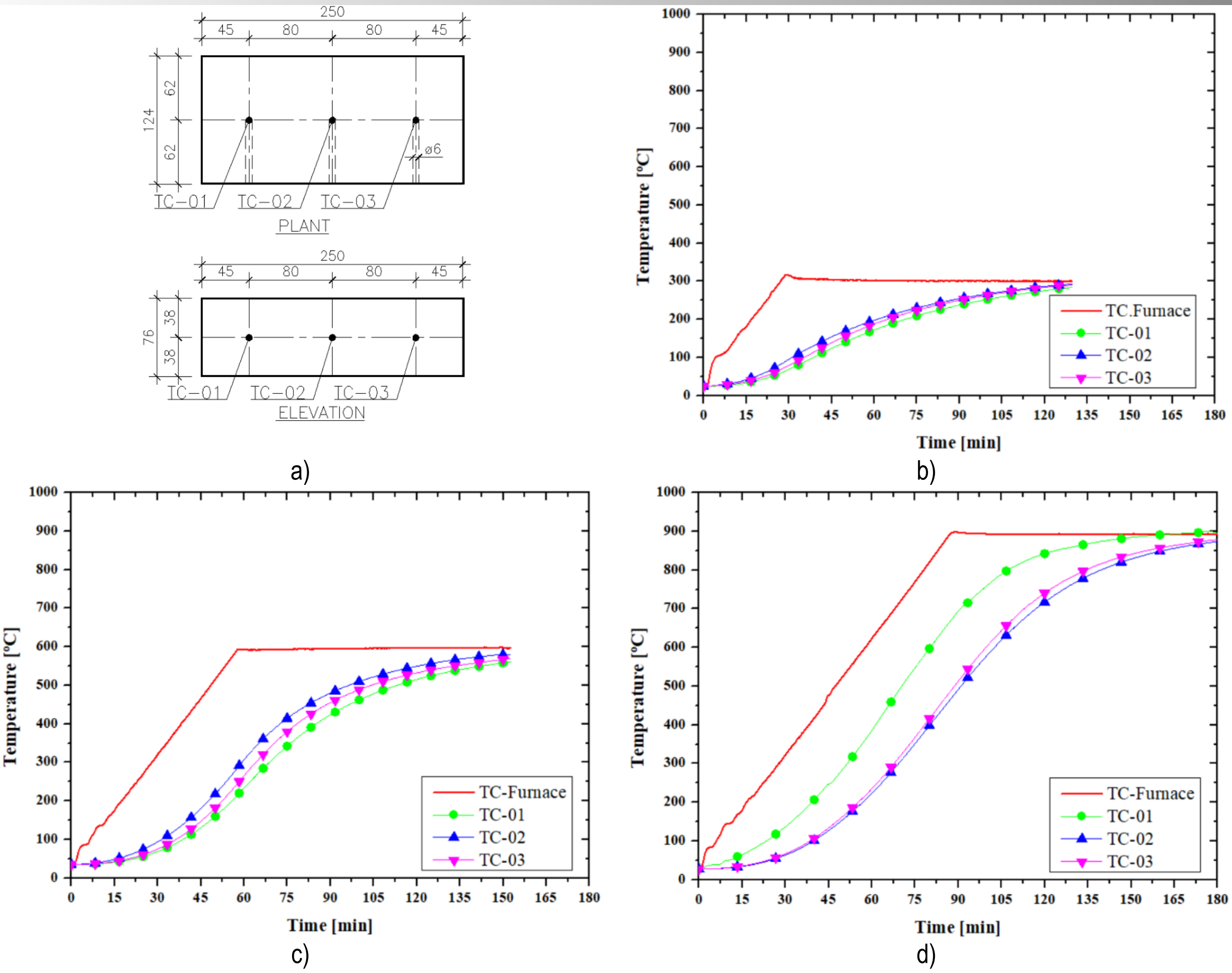

Figure 19 – Slip test: a) Thermocouple position, b) Temperatures of specimen ST.300.01, c) Temperature of specimen ST.600.01 and d) Temperature of specimen ST.900.01.

The experimental procedure had the following steps: *i*) The bricks were placed at the inclinable beam and the instrumentation (LVDT and thermocouples) was installed; *ii*) The furnace was set to heat at 10 ºC/min; *iii*) When the temperature test was reached, a dwell time of 90 minutes was applied; *iv*) The hydraulic jack was set to move upward at a rate of 0.5 mm/s, up to the maximum of 170 mm; *v*) When the upper brick slips, according to the LVDT cables installed, the displacement of the hydraulic jack was recorded; *vi*) The friction angle was calculated based on the displacement of the hydraulic jack and the offset between the hinge axis and the hydraulic jack axis, as shown in Equ. 2.

3.2.2 Results and discussion

Figure 20 shows the displacement curves for the different temperatures. The curves of the graphs are from the first specimen among the tests carried out. Six specimens were tested at ambient temperature and three at each subsequent temperature. The displacements were measured in the hydraulic jack (jack's LVDT) and the brick (cable LVDT) (Oliveira *et al*, 2021).

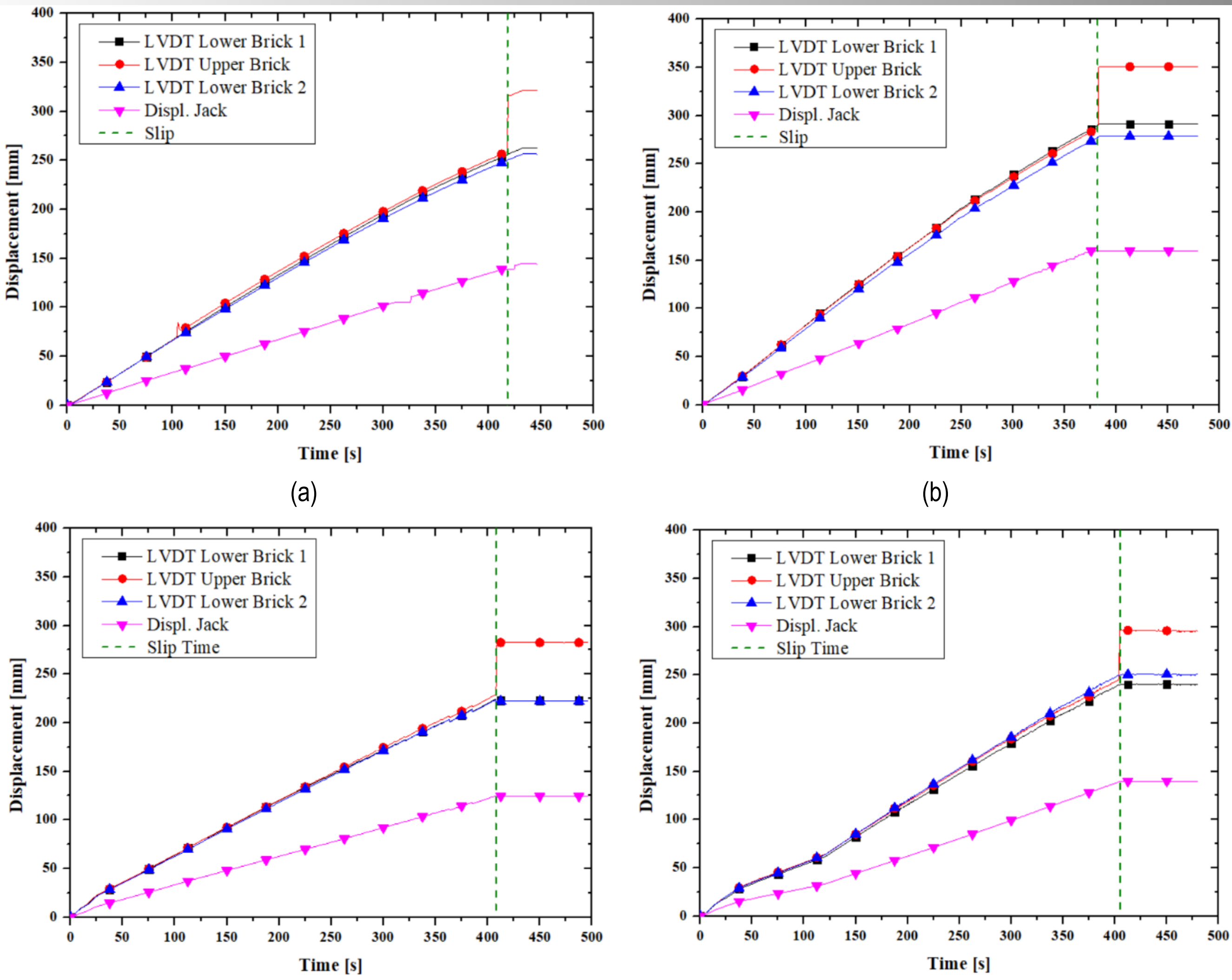

(a) (b)

(c) (d)

Figure 20 – Displacements: a) ambient temperature, b) 300 ºC, c) 600 ºC and d) 900 ºC.

The slip test results for ambient temperature, 300 ºC, 600 ºC and 900 ºC are presented in Table 2. The friction angle (ø), friction coefficient (μ) and the standard deviations are also presented. The average friction angle at ambient temperature is 30.9º. The friction angle at 300 ºC was 26.5º that is below the value at ambient temperature. However, a small increase is observed for higher temperatures when compared with the value at 300 ºC, being 27.0º for 600 ºC and 27.9º for 900 ºC (Figure 21). The reduction of the friction coefficient when compared to the ambient temperature results was 14.2 %, 12.6 % and 9.7 % for the temperatures of 300 ºC, 600 ºC and 900 ºC, respectively. A small standard deviation was found for all test series. The final configuration of the specimens before and after the tests are shown in Figure 22. The slipping of the bricks occurred as expected, the brick did not touch the lateral steel pieces used to protect the heating elements of the furnace.

Table 2 – Results of the slip tests at ambient and high temperatures.

Test series	Temperature	Specimen	Hydraulic jack displacement [mm]	Horizontal offset [mm]	ø [°]	μ [-]	$ø_{avg}$ [°]	σ (ø) [°]	$μ_{avg}$ [-]	σ (μ) [-]
ST.RT	20 °C	ST.RT.01A	138.9	240.0	30.06	0.58	30.9	0.78	0.598	0.02
		ST.RT.01B	143.6	240.0	30.89	0.60				
		ST.RT.01C	147.8	240.0	31.63	0.62				
		ST.RT.02A	139.1	240.0	30.10	0.58				
		ST.RT.02B	146.6	240.0	31.42	0.61				
		ST.RT.02C	135.5	240.0	29.45	0.56				
ST.300	300 °C	ST.300.01	119.1	240.0	26.39	0.50	26.5	0.49	0.498	0.01
		ST.300.02	122.8	240.0	27.10	0.51				
		ST.300.03	116.6	240.0	25.91	0.49				
ST.600	600 °C	ST.600.01	124.8	240.0	27.47	0.52	27.0	0.55	0.510	0.01
		ST.600.02	118.4	240.0	26.26	0.49				
		ST.600.03	124.2	240.0	27.36	0.52				
ST.900	900 °C	ST.900.01	133.4	240.0	29.07	0.56	27.9	1.17	0.530	0.03
		ST.900.02	129.4	240.0	28.33	0.54				
		ST.900.03	118.6	240.0	26.30	0.49				

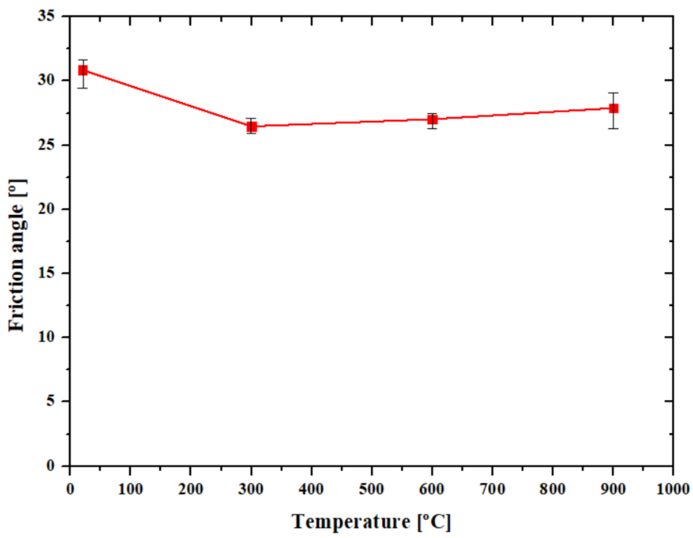

Figure 21 – Evolution of the friction angle versus temperature.

a) b)

Figure 22 – Slip test specimens: a) Beginning of the test and b) After slipping.

4 Joint with mortar

4.1 Experimental setup

Masonry systems with mortar joints are composed of bricks, mortar joints and the brick-mortar interface. The latter represents the interaction behaviour between the bricks and the mortar joints. The brick-mortar interface is usually considered as the weakest link in the masonry with mortar structure. Therefore, it's behaviour is widely investigated under tensile and shear loads to obtain its failure criteria in terms of ultimate tensile strength (f_t) , cohesion (C), internal friction angle (ϕ) as well as other parameters. Shear failure of the brick-mortar interface is considered as a major collapse mechanism of masonry systems. Usually, shear loads are combined with compression or tensile loads. Therefore, in experimental investigations, pure shear modes are changed either to shear tension or shear compression modes. The shear strength of the brick-mortar interface depends on the applied normal stress to the interface.

To determine Φ and C, the normal and shear stresses, until failure of the brick-mortar interface, should be measured.

The main challenge in performing shear tests is maintaining a uniform stress state in the mortar joints. Several studies were carried out to develop a test setup and to characterize the shear behaviour of brick mortar interface at room (Van der Pluijm 1993; Van Der Pluijm 1997; Alecci et al. 2013; Lourenço, Barros, and Oliveira 2004; Atkinson et al. 1989) and high temperature (Brulin et al. 2020). Brulin et al. 2020 developed a slanted shear test setup to characterize the shear behaviour of refractory brick-mortar interface at room and high temperatures. In the present work, a similar test setup to the one developed by Brulin et al. was used to characterize the shear failure criteria of refractory brick-mortar interface. The experimental setups used to measure the shear failure criteria at room and high temperatures are shown in Figure 23. They are composed of a universal testing machine, a load cell for measuring the applied load, a computer for data and images recording, a CCD camera for taking pictures of the specimen and a furnace equipped with a glass window (for high temperature tests only).

European Commission
Horizon 2020
European Union funding
for Research & Innovation

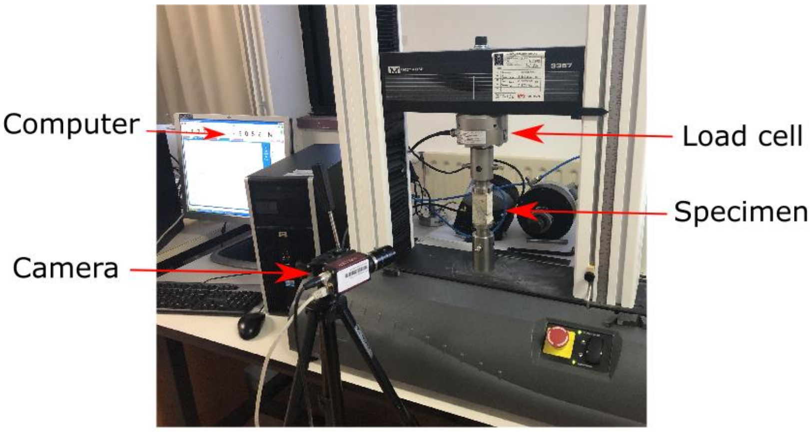

a)

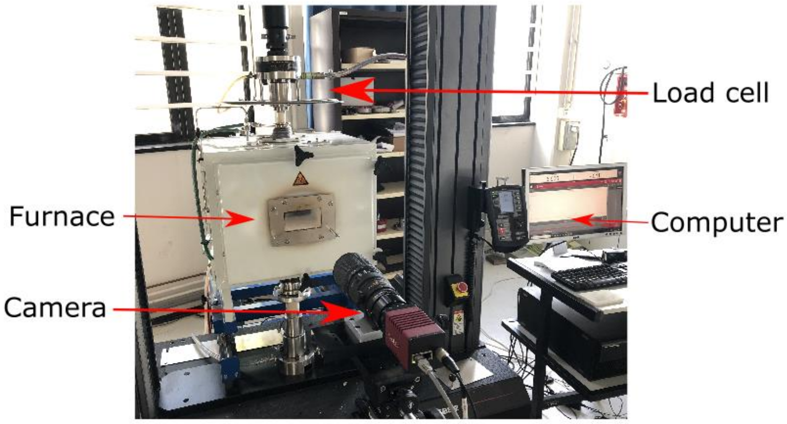

b)

Figure 23 – Slanted shear test experimental setups used for the characterization of refractory brick-mortar interface at a) ambient and b) high temperatures.

A schematic of slanted shear test specimen is shown in Figure 24. Two wedge shaped bricks are glued together by an inclined mortar joint. The main advantage of this specimen design is that it is possible to apply normal and shear stresses at the brick – mortar interface with a standard compression testing machine. The local normal compression σ_n and shear τ stresses applied on the brick - mortar interface can be written in terms of the inclination angle of the joint and the applied average stress as following:

$$\begin{cases} \sigma_n = \sigma \cdot \cos^2 \alpha \\ \tau = \sigma \cdot \cos \alpha \sin \alpha \end{cases} \quad \textbf{Equ. 3}$$

Where, σ is the global homogeneous applied compression stress and α is the angle between the mortar joint and the plane normal to the compression loading axis (see Figure 23). The applied average compression stress is computed by dividing the applied force (F) by the cross-section area (A) of the specimen ($\sigma = F/A$).

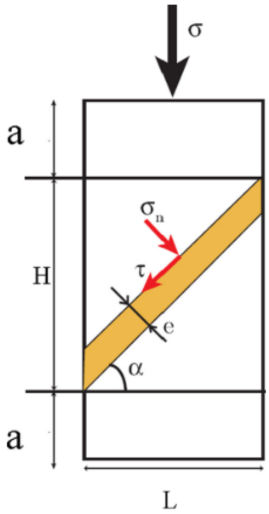

Figure 24 - Schematic of slanted shear test specimen (Brulin et al. 2020).

To determine the shear failure criteria of the brick-mortar interface (i.e. the cohesion and the internal friction angle), at least three samples with three different joint angles (α) are required. The experimental tests of the three samples will produce three points which are the minimum to produce a good line. The choice of the angles is driven by characteristics of the experimental setup such as furnace dimensions, mechanical constrains and load cell capacity. A good choice of α would maximize the ratio between resulting shear and normal stress at the brick -mortar interface. Using Equ. 3, the variations of the normalized normal and shear stresses at the brick-mortar interface with α are calculated. These variations are shown in Figure 25. It can be seen from this figure that a good value of α should be higher than or equal to 45°. Therefore, in the present work, three joint inclination angles are chosen: 45°, 55° and 65°. It should be noted that the total height of the specimen increases with the increase of the inclination angles. The dimensions of specimens with the three chosen angles are depicted in Figure 26. In all cases, the cross-section area of the specimen is $35 \times 35\ mm^2$ and the thickness of the mortar joint is 2 mm.

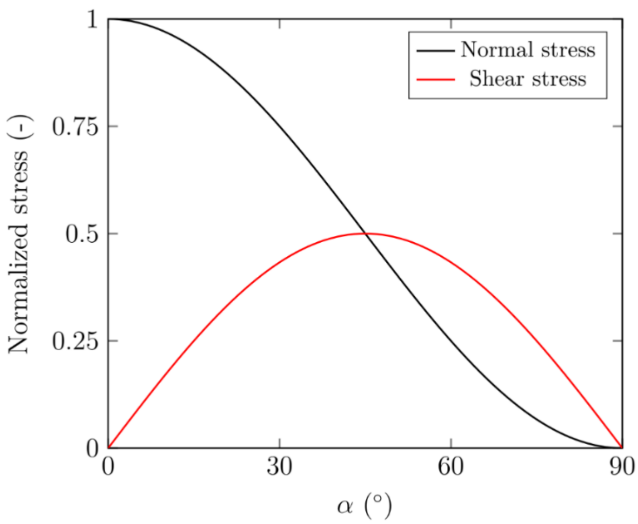

Figure 25 - Normal and shear stresses at the brick-mortar interface variation as a function of mortar joint inclination angle (α).

European Commission
Horizon 2020
European Union funding
for Research & Innovation

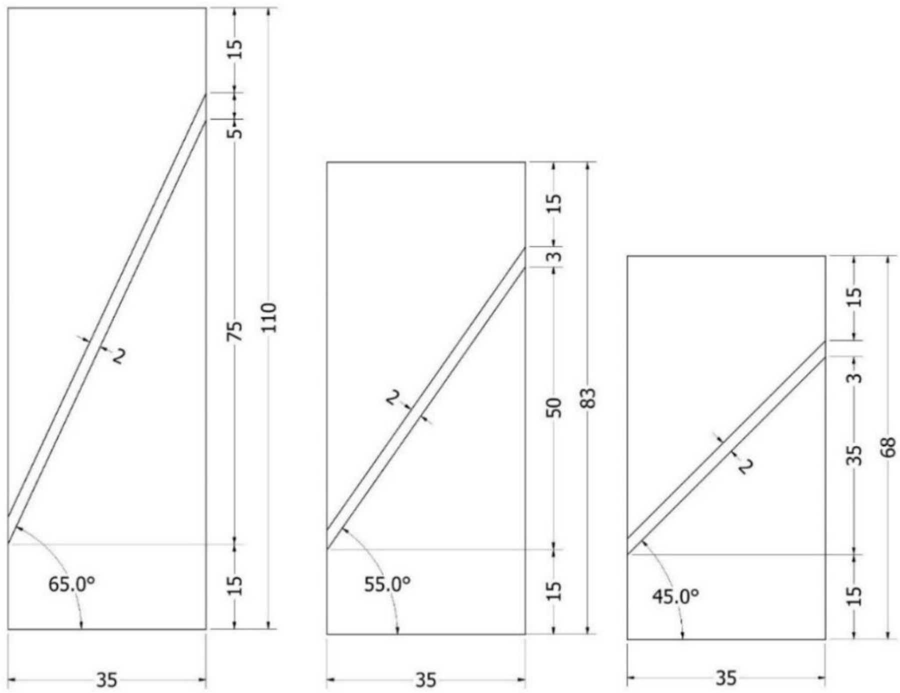

a) b) c)

Figure 26 - Dimensions of slanted shear tests specimen: a) α = 65 °, b) = 55 ° and c) = 45 °. Dimensions are in mm.

Two refractory brick materials and one ready to use mortar are used to produce the samples. The first type of sample is made of two wedge shaped bauxite bricks glued together with one air hardening mortar joint. The second type of samples is made of two wedge shaped chamotte bricks glued together with one air hardening mortar joint. The air hardening mortar is ready to use mortar (i.e. the required amount of water was added previously by the producer). The two types of the refractory bricks and the mortar material tested in the present work are used to build the safety lining of the industrial scale steel ladle studied within the framework of ATHOR project.

The wedge shaped bricks are cut, from commercial size bricks, using a saw. Then, green mortar was shaped between the two wedge shaped samples, followed by hardening at room temperature during 48 h and drying at 110 °C during 24 h. The tests were performed on a universal testing machine with a standard compression device with displacement control. The displacement speed rate was tuned to 0.5 mm/min. Summary of the bauxite and chamotte test series are given in Table 3 and Table 4, respectively. For each test series, the test was repeated at least two times. For specimens with bauxite bricks, the tests are performed at ambient temperature and 600 °C. Chamotte specimens are tested at ambient temperature.

Table 3 – Summary of performed slanted shear tests of bauxite bricks and air hardening mortar.

Test series	Specimen	Material	Angle	Temperature
BX-45-RT	BX–45 –RT-01	Bauxite	45	Room temp
	BX–45 –RT-02			
	BX–45 –RT-03			
BX-55-RT	BX–55 –RT-01	Bauxite	55	
	BX–55 –RT-02			
	BX–55 –RT-03			
BX-65-RT	BX–65 –RT-01	Bauxite	65	
	BX–65 –RT-02			
	BX–65 –RT-03			
BX-45-600	BX–45 –600-01	Bauxite	45	600 °C
	BX–45 –600-02			
	BX–45 –600-03			
BX-55-600	BX–55 –600-01	Bauxite	55	
	BX–55 –600-02			
	BX–55 –600-03			
BX-65-600	BX–65 –600-01	Bauxite	65	
	BX–65 –600-02			

Table 4 – Summary of performed slanted shear tests of chamotte bricks and air hardening mortar.

Test series	Specimen	Material	Angle	Temperature
Ch-45-RT	Ch –45 –RT-01	Chamotte	45	Room temp
	Ch –45 –RT-02			
	Ch –45 –RT-03			
Ch -55-RT	Ch –55 –RT-01	Chamotte	55	
	Ch –55 –RT-02			
	Ch –55 –RT-03			
Ch -65-RT	Ch –65 –RT-01	Chamotte	65	
	Ch –65 –RT-02			
	Ch –65 –RT-03			
	BX–65 –600-02			
	BX–65 –600-03			

4.2 Results and discussion

Figure 27 shows a bauxite specimen with $\alpha = 65°$ before testing, during and after failure (at room temperature). Figure 28 presents bauxite specimens with different joint inclination angles (α) after testing at room temperature. It can be seen from the two figures that the cracks are located at the interface between the mortar joint and the wedge-shaped bricks. Similar failure modes are obtained for bauxite specimens tested at 600 °C as well as chamotte specimens tested at room temperature. Therefore, for all tested materials the global failure mode can be considered as failure of the brick mortar interface.

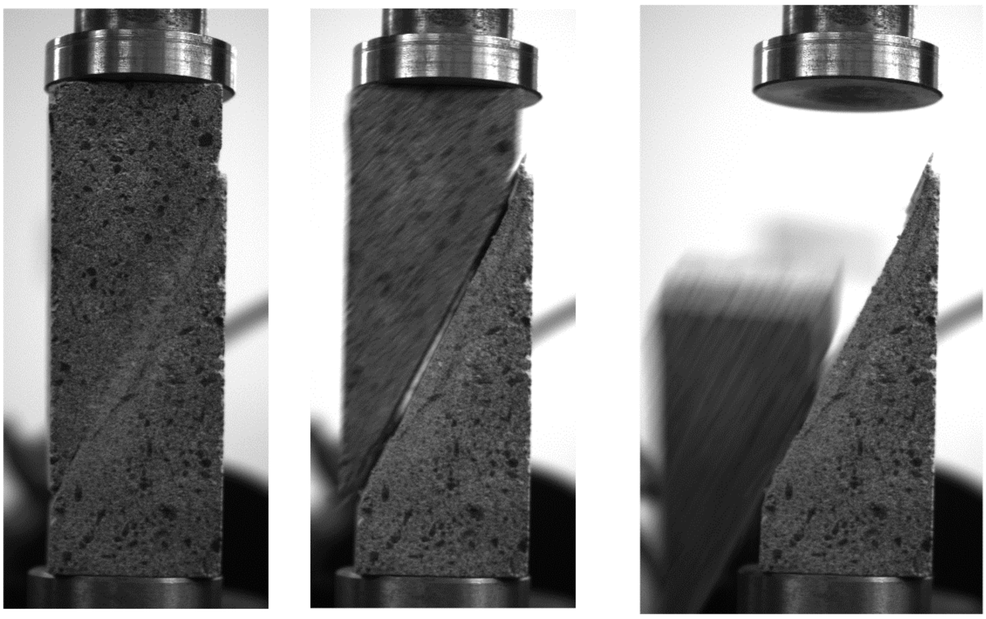

a) b) c)

Figure 27 - Slanted shear test specimen a) before testing, b) during failure and c) after failure.

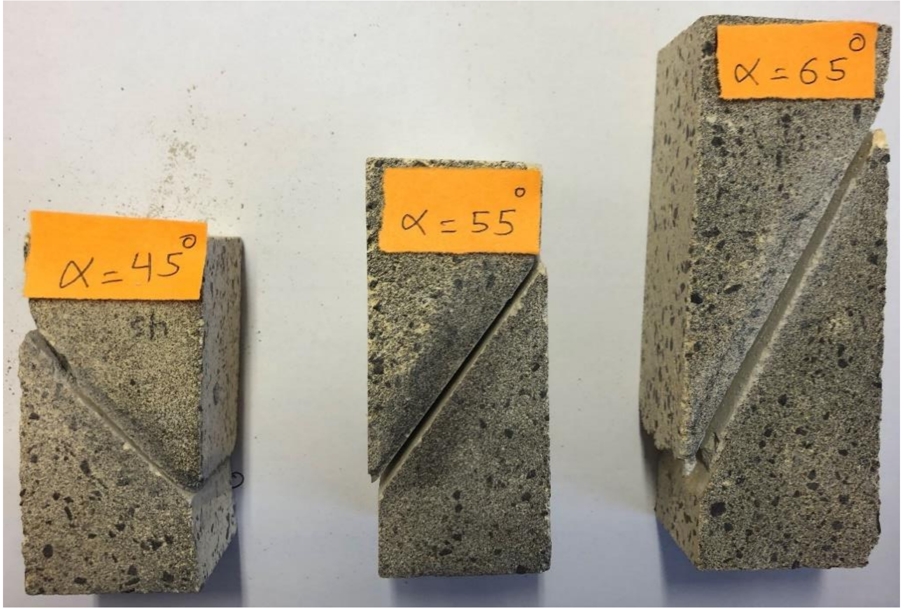

Figure 28 - Slanted shear test specimens with different inclination angles (α) after testing.

The vertical strain field in bauxite specimens with a joint inclination angle of 45° determined using digital image correlation technique is presented in Figure 29. The image corresponds to the maximum load level corresponding to fracture (10500 N). It can be seen that the maximum compressive strain is located in the mortar joint. It is due to the fact that the Young's modulus of the mortar is smaller than that of the brick.

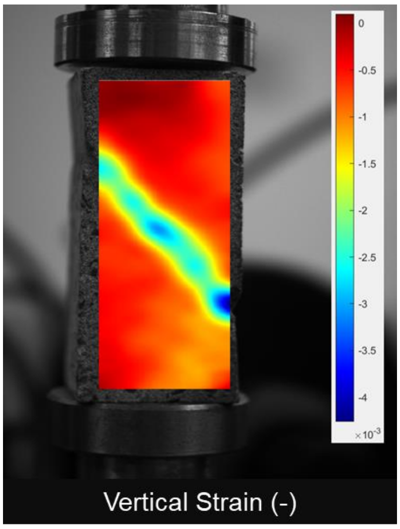

Figure 29 – Vertical strain field in Bauxite specimen with α = 45°.

Figure 30 shows typical load versus displacement curves obtained during the test of bauxite specimen. The different curves correspond to the three different joint inclination angles tested at room temperature. The maximum load (corresponding to fracture) decreases with the increase of mortar joint's inclination angle. From the maximum load corresponding to fracture and using Equ. 3, the resulting maximum normal and shear stresses at the brick mortar interface can be determined.

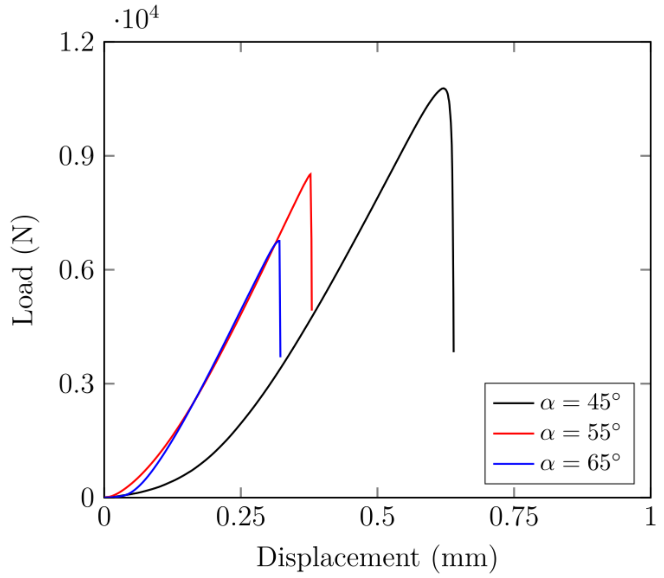

Figure 30 - Load versus displacement curves for bauxite specimens with different inclination angles (α).

Using the maximum resulting normal and shear stresses at the brick mortar interface, it is possible to draw the Mohr-Coulomb lines. The resulting normal and shear stresses extracted from the load versus displacement curves of bauxite specimens at room temperature and 600 °C are given in Figure 31. The resulting normal and shear stresses extracted from the load versus displacement curves of chamotte specimens at room temperature are shown in Figure 32. By fitting the experimental data, the Mohr-Coulomb line can be obtained. The shear failure criteria, cohesion and internal friction angle, for each temperature can be determined from this line. For bauxite specimens. at room temperature the value of the cohesion is equal to 0.73 MPa, while it is equal to 1.26 MPa at 600 °C. The internal friction angles are 41° and 40.3° at room temperature and 600 °C, respectively. Regarding chamotte specimens, the cohesion and internal friction angle at room temperature are equal to 0.96 MPa and 39.7 °, respectively.

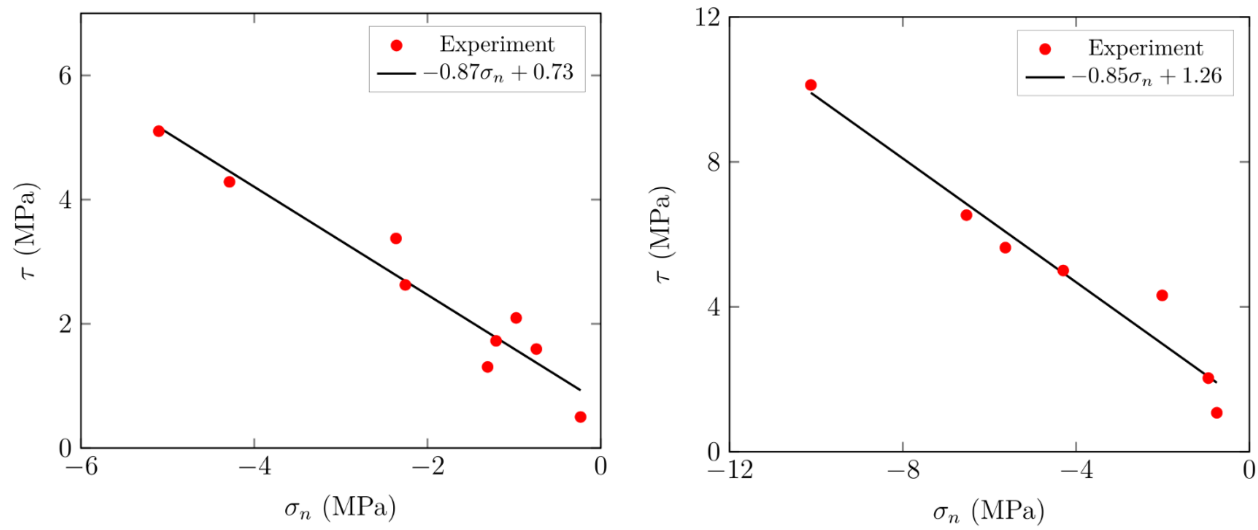

a) b)

Figure 31 - Mohr-Coulomb lines for bauxite specimens at a) room temperature and b) 600 °C.

European Commission
Horizon 2020
European Union funding
for Research & Innovation

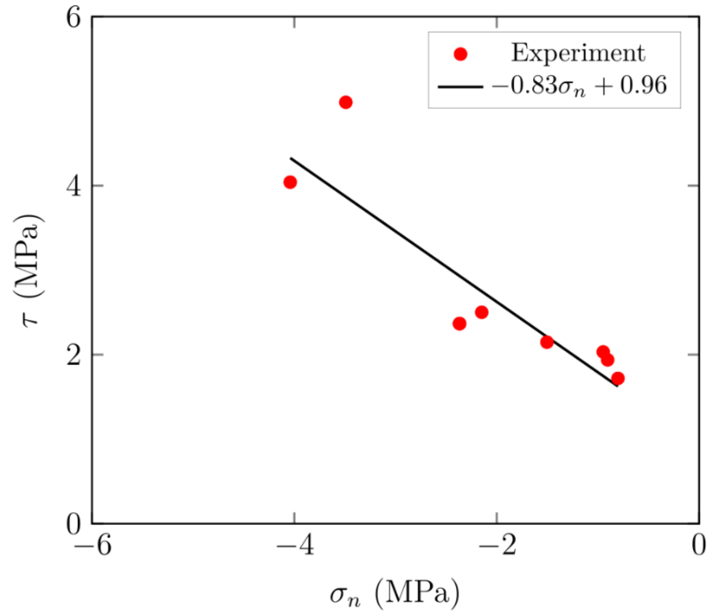

Figure 32 - Mohr-Coulomb lines for chamotte specimens at room temperature.

5 Conclusion

This document gathers the results of experimental campaigns on masonry joints. Both dry joints (without mortar) and joint with mortar were studied.

Joints without mortar (for alumina-spinel bricks corresponding to the working lining) were studied for both normal and shear behaviour. A classical joint closure test was performed in two stacked bricks and compared to joint closure measurements on a refractory wallet measured by DIC. It was observed that the heterogeneity on the joint closure was higher in the masonry wallet. In the latter case, the geometric imperfections in a full course influence the contact conditions of the bricks, resulting in joints with higher heterogeneity and compressibility. Classical joint closure tests were also performed at different temperatures (600 ºC, 800 ºC, 1000 ºC and 1200 ºC), and it was found that the contact pressure required to close the joint decreased with the increase in temperature, this behaviour is explained by the reduction in the elastic modulus of the material at higher temperature. A novel test setup, for evaluating the friction coefficient between bricks in dry joints, was developed and presented. The equipment was used to evaluate the friction coefficient of the alumina spinel bricks at ambient temperature, 300 ºC, 600 ºC and 900 ºC. A reduction of the friction coefficient was found when subjected to high temperatures.

Concerning joints with mortar (for bricks corresponding to the safety lining), slanted shear tests at room and high temperature were performed to characterize the shear failure criteria of the refractory brick-mortar interface. Two refractory brick materials and one ready to use mortar have been tested. The two refractory materials are bauxite and chamotte, while air hardening mortar was used to glue the refractory bricks together to produce the samples. From the first obtained results, it has been shown that similar values of the internal friction angle are obtained at room and high temperature. However, higher values of cohesion are obtained at high temperature. Further investigations are ongoing and will lead to an update of this deliverable in a couple of months.

6 References

Alecci, Valerio, Mario Fagone, Tommaso Rotunno, and Mario De Stefano. 2013. "Shear Strength of Brick Masonry Walls Assembled with Different Types of Mortar." *Construction and Building Materials* 40, pp 1038–1045.

Allaoui, S.; Rekik, A.; Gasser, A., Blond, E.: Andreev, K. "Digital Image Correlation measurements of mortarless joint closure in refractory masonries". Construction and Building Materials, vol. 162, 2018, pp. 334-344

Andreev, K.; Sinnema, S.; Rekik, A.; Allaoui, S.; Blond, E.; Gasser, A. "Compressive behaviour of dry joints in refractory ceramic masonry". Construction and Building Materials, vol. 34, 2012, pp. 402-408

Atkinson, R. H., B. P. Amadei, S. Saeb, and S. Sture. 1989. "Response of Masonry Bed Joints in Direct Shear." *Journal of Structural Engineering* 115 (9), pp 2276–2296

Brulin, J.; Blond, E.; Bilbao, E.; Rekik, A.; Landreau, M.; Gasser, A.; Colleville, Y. "Methodology for brick/mortar interface strength characterization at high temperature" Construction and Building Materials. vol. 265, 2020, 120565

European Committee for Standardization (CEN)(2002) Methods of test for masonry - Part 3: Determination of initial shear strength, EN 1052-3, Brussels: CEN.

Gasser, A.; Terny-Rebeyrotte, K.; Boisse, P. “Modelling of joint effects on refractory lining behaviour”. Journal of Materials: Design and Applications, vol. 218, issue 1, 2004, pp.19-28.

Lourenço, P.B., J.O. Barros, and J.T. Oliveira. 2004. “Shear Testing of Stack Bonded Masonry.” *Construction and Building Materials* 18 (2), pp 125–32.

Nguyen, T.; Blond, E.; Gasser, A.; Prietl; T. “Mechanical homogenisation of masonry wall without mortar”. European Journal of Mechanics - A/Solids. vol. 28, Issue 3, 2009, pp. 535-544.

Oliveira, R.; Rodrigues J. P.; Pereira, J. M. “The Characterization of joint Behaviour in Mortarless Refractory Masonry”. In Proceedings of the Unified International Technical Conference of Refractories, Yokohama, Japan, 2019, pp. 612-614

Oliveira, R; Rodrigues, J. P.; Pereira, J, M.; Lourenço, P. B.; Marschall, H. U. “Normal and tangential behaviour of dry joints in refractory masonry” Engineering Structures. Vol. 243, 2021, 112600

Prietl, T., “Ermittlung materialspezifischer Kennwerte von feuerfesten Werkstoffen und Zustellungen unter uni- und biaxialen Lastbedingungen für die Nichteisenmetallindustrie,” PhD Thesis, University of Leoben, 2006, 192 pages.

Prietl, T.; Zach, O.; Studnicka, H. “The evaluation of refractory linings thermomechanical properties”. Erzmetall – World of metallurgy, 59, 2006, pp. 127–132

Van der Pluijm, R. 1993. “Shear Behaviour of Bed Joints.” In *Proceedings of the 6th North American Masonry Conference. Drexel University, Philadelphia, Pennsylvania, USA*, 125–36.

Van der Pluijm, R. 1997. “Non-Linear Behaviour of Masonry under Tension.” *Heron* 42 (1), pp 25–48.